Carbohydrate Polymers 183 (2018) 294–302

Contents lists available at ScienceDirect

Carbohydrate Polymers

journal homepage: www.elsevier.com/locate/carbpol

Production of cellulose nanoparticles from blue agave waste treated with environmentally friendly processes

Eduardo Robles[a], Javier Fernández-Rodríguez[a], Ananda M. Barbosa[a,b], Oihana Gordobil[a], Neftali L.V. Carreño[b], Jalel Labidi[a,*]

[a] Biorefinery Processes Research Group, Chemical & Environmental Engineering Department, University of the Basque Country UPV/EHU, Plaza Europa 1, 20018, Donostia, Spain

[b] Materials Science and Engineering, Technology Development Center, Federal University of Pelotas, Gomes Carneiro 1, 96010610, Pelotas, RS, Brazil

ARTICLE INFO

Keywords:
Blue agave
Organosolv
Cellulose nanocrystals
Cellulose nanofibers

ABSTRACT

Tequila elaboration leaves two main byproducts that are undervalued (bagasse and leaves). Organosolv pulping and Total Chlorine Free bleaching were integrated to obtain cellulose fibers from agricultural waste which consisted of blue agave bagasse and leaf fibers; together they represent a green process which valorizes biomass waste. The obtained celluloses were characterized by FT-IR, colorimetry, and SEM and their extraction yields were evaluated. These celluloses were used to produce cellulose nanocrystals and cellulose nanofibers. First, an acid hydrolysis was performed in a sonication bath to induce cavitation during the reaction to produce cellulose nanocrystals. Then a high-pressure homogenization was selected to produce cellulose nanofibers. These nanocelluloses were characterized by powder XRD, Nanosizer, zeta potential, NMR, and electronic microscopy. Results showed that cellulose from organosolv pulps bleached with TCF bleaching is suitable for nanocellulose production. Moreover, the use of a new step to separate cellulose nanocrystals resulted in yields almost doubling traditional yields, while the rest of the properties remained within the expected.

1. Introduction

Blue agave (*Agave tequilana* Weber var. azul) is one of the most abundant agricultural products in Mexico, in which tequila is produced from this plant. The core of the plant represents up to 54% on a wet weight basis (Iñiguez-Covarrubias, Díaz-Teres, Sanjuan-Dueñas, Anzaldo-Hernández, & Rowell, 2001) of the blue agave plant and is cooked and milled for tequila production. Bagasse is the residue left after the core is cooked, shredded and milled thus being an undervalued by-product with a high amount of cellulose and lignin. Leaves can be up to 36% and are in general left in the field after being cut yearly (*Jima* in Mexican Spanish); this trimming is done annually to enhance the growth of the core while most of the leaves are cut during the core harvesting. Total year production was (in thousands of tons) 788.2 in 2014, 788.9 in 2015 and 941.8 in 2016 as stated by the Tequila Council (National Regulator Council for Tequila Industry, 2017).The management of the waste of tequila industry has attracted the interest of researchers, and the obtention of value-added products from blue agave wastes has proved the suitability of such raw material as a lignocellulosic source (Fernández-Rodríguez, Gordobil, Robles, González-Alriols, & Labidi, 2017; Tronc et al., 2007). Pulp for paper has been obtained from blue agave having similar properties than those of commercial paper (Idarraga, Ramos, Zuñiga, Sahin, & Young, 1999; Iñiguez-Covarrubias et al., 2001).

Removal of lignin from lignocellulosic fibers is the first step in the obtention of cellulose. Industrially, cellulose pulp is obtained using two stages: pulping and bleaching. The most commonly used method is the Kraft process, which provides high pulp yields, but can generate sulfide derivatives that may be linked to cellulose and represent an environmental problem during disposal. In this sense, environmental friendly pulping processes have emerged in last decades, such as organosolv (O_T) methods. Moreover, the organosolv process is a sulfur-free method, based on the extraction of lignin by its dissolution in organic solvents at high temperature and pressure, the low viscosity of the organosolv white liquors favors the penetration into the fibers, allowing that a high lignin fraction can be dissolved. Moreover, after the pulping stage, the solvent could be recovered by distillation (Fernández-Rodríguez et al., 2017).

After pulping, some residual lignin remains in the fibers and is usually removed in oxidative bleaching reactions. For many years, the

* Corresponding author.
E-mail addresses: joseeduardo.robles@ehu.eus (E. Robles), javier.fernandezr@ehu.eus (J. Fernández-Rodríguez), ananda.barbosa@ufpel.edu.br (A.M. Barbosa), oihana.gordobil@ehu.eus (O. Gordobil), neftali@ufpel.edu.br (N.L.V. Carreño), jalel.labidi@ehu.eus (J. Labidi).

https://doi.org/10.1016/j.carbpol.2018.01.015
Received 10 October 2017; Received in revised form 3 January 2018; Accepted 5 January 2018
Available online 06 January 2018
0144-8617/

main bleaching reactions have involved chlorinated reagents (Cl_2, ClO_2, and NaOCl), but nowadays chlorine is avoided in most pulp types because of its negative environmental effects (Bajpai, 2004; Fillat et al., 2017; Nelson, 1998).Current bleaching sequences include the use of chlorine dioxide in Elemental Chlorine-Free (ECF) sequences (Gierer, 1982; Lachenal et al., 2005; Mateo, Chirat, & Lachenal, 2005). The other family of bleaching sequences is the Total Chlorine Free (TCF) bleaching, which avoids releasing chlorine derivates into the waste streams or atmosphere. Residual lignin degradation with hydrogen peroxide is based on the action of the radicals produced during single electron transfers between hydrogen peroxide and catalysts or as a result of thermal cleavage of the oxygen−oxygen bond (Gellerstedt & Pettersson, 1982; Gierer, 1982; Süss & Nimmerfroh, 1996). Some approaches have been made to assembly organic-based pulping with TCF bleaching sequences to develop greener cellulose-extraction processes (Alonso, Parajó, & Yáñez, 2003; Shatalov & Pereira, 2007), however, so far these researchers have included the use of chemicals (acetic acid, HCl, anthraquinone, methanol, etc.) which may fit within the organosolv processes (organic solvent) but not in the environmentally-friendly processes, therefore the present study aims to integrate an ethanol-water organosolv pulping with a TCF bleaching to obtain a fully green cellulose pulp.

Recent studies have been focused on developing micro and nanoscale cellulosic materials trying to reduce the size of the cellulose fibers to a size range in which their properties vary considerably. These materials have wide applications as can be biomedicine, pharmacy and materials science (Aranda-García, González-Núñez, Jasso-Gastinel, & Mendizábal, 2015; García, Gandini, Labidi, Belgacem, & Bras, 2016; Gatenholm & Klemm, 2010; Henriksson, Henriksson, Berglund, & Lindström, 2007; Lavoine, Desloges, Dufresne, & Bras, 2012). Nanocellulose production can be achieved either by mechanical treatments, (Chen et al., 2011; Hettrich, Pinnow, Volkert, Passauer, & Fischer, 2014; Iwamoto, Abe, & Yano, 2008; Lee, Chun, Kang, & Park, 2009); chemical processes (Herrera, Téllez-Luis, González-Cabriales, Ramírez, & Vázquez, 2004; Morán, Alvarez, Cyras, & Vázquez, 2008); or by enzymatic techniques; or even combinations of the above (Eichhorn, 2011; Jonoobi, Harun, Shakeri, Misra, & Oksman, 2009). For blue agave byproducts, cellulose nanofibers (Ponce-Reyes et al., 2014; Robles, Salaberria, Herrera, Fernandes, & Labidi, 2016)and cellulose nanocrystals (Espino et al., 2014) have been produced and used in diverse applications, but the specific properties of cellulose nanoparticles from blue agave have not been fully studied yet.

In this research, the production of cellulose nanoparticles from two side-streams from tequila production (blue agave bagasse and leaves) was studied to give value-added to these materials. Two main innovations were made regarding previous works. The first part of the work was focused on the use of a fully environmentally-friendly process for the separation of the cellulose fibers from the original biomass by combining an organosolv pulping and a TCF bleaching sequence, both of which have not yet been fully studied as an assembly. Afterwards, two different methods were followed to produce nanocellulosic products: nanofibers and nanocrystals. The second being a sonochemical hydrolysis in acid media to produce cellulose nanocrystals (CNC), with the introduction of a physical particle separation method which provides better yields and homogeneousness than traditional centrifuge-based particle separation. Mechanical defibrillation with high-pressure homogenization (HPH) was used to produce cellulose nanofibers (CNF). The obtained nanoparticles were analyzed in their physicochemical properties to determine the potential valorization of these byproducts into high value-added cellulose nanoparticles.

2. Experimental

2.1. Materials

Blue agave (*Agave tequilana* Weber var. azul) leaves and bagasse fibers, which were provided by Finca Noctitlan, Jalisco, Mexico, were used as feedstock in this work. Leaves were cut mature fresh from the plant and then decorticated to scrape off the epidermis and pithy material from the line fiber and then rinsed and dried. Bagasse was collected after core cooking and milling and was also rinsed and dried.

2.2. Cellulose isolation

2.2.1. Organosolv delignification treatment

An ethanol-water (70:30 v/v) organosolv treatment (O_T) was carried out in order to extract lignin from fibers; the method followed according to the chemical composition of the raw material: temperature was set at 200 °C with pressure being stabilized at ~30 bar; agitation was set at 150 rpm and the reaction was performed during 90 min (Gordobil, Egüés, Llano-Ponte, & Labidi, 2014). Liquid fraction was separated via filtration and the solid fraction was washed several times until remaining black liquor was eliminated.

2.2.2. Total chlorine-free bleaching

An industrial type of Total Chlorine Free bleaching process was performed on the pretreated fibers (Ibarra, Camarero, Romero, Martínez, & Martínez, 2006). In the present work, TCF sequence was done as follows: (1) Alkali oxygen stage (O_2) performed twice, with water at pH 11 stabilized using NaOH and 0.2 wt% $MgSO_4$ to neutralize remaining metals, this was performed under a 6 bar oxygen atmosphere at 98 °C during 60 min. (2) Peroxide stage with a secondary chelating reaction (P_Q) using 3 M H_2O_2, at pH 11 with 1:5 (w/v) pentetic acid (DTPA) as chelant, reaction was performed for 120 min at 105 °C and (3) alkaline peroxide stage (P_O) using a 3 M H_2O_2 solution at pH 11 and 0.2 wt% $MgSO_4$ at 98 °C during 150 min under 6 bar O_2 atmosphere. Bleached pulp was washed several times until neutral pH after each stage and then oven dried at 50 °C for 24 h (Li, Lee, Lee, & Youn, 2011). Pulping and bleaching were carried out in a 4 L stainless steel batch reactor with electronically controlled stirring, pressure, and temperature.

2.3. Nanocellulose production

2.3.1. Cellulose preparation

Prior to elaborating cellulose nanofibers or cellulose nanocrystals, bleached cellulose fibers were milled with a Retsch mill using a 1 mm sieve and then kept inside a conditioning chamber with no humidity at 25 °C.

2.3.2. Sonochemical acid hydrolysis enhanced with sonication

Acid hydrolysis was performed to cellulose by using 10.2 M H_2SO_4 (1:15 w/v) solution at 45 °C during 60 min inside an Elmasonic Elma S 70 H sonication bath as present in Fig. 1. In this process, cavitations were induced at 37 kHz, the use of cavitations during hydrolysis as an incorporated process instead of being a 2-step process is a recent approach which has proven to produce more homogeneous CNC while reducing production times(Barbosa et al., 2016; Guo, Guo, Wang, & Yin, 2016). The reaction was stopped with cold distilled water (1:3 v/v), the non-hydrolyzed fraction was separated with a sintered glass Buchner-funnel (grain No.1), after which the filtrate was concentrated and washed twice by using a nylon membrane (0.45 μm) combined with a sintered glass Buchner-funnel (grain No. 3) obtaining a wet mat which was dispersed in distilled water to a 10 wt% and a pH of 5. CNC were further dialyzed to distilled water until neutral pH was stabilized. CNC suspension was adjusted to a 3 wt% solution by direct sonication for 10 min at 20 °C and kept at 5 °C (Garcia de Rodriguez, Thielemans, & Dufresne, 2006).

2.3.3. Mechanical defibrillation

Cellulose nanofibers were produced with a Niro-Soavi Panda high-pressure homogenizer; milled fibers were first dispersed in a water

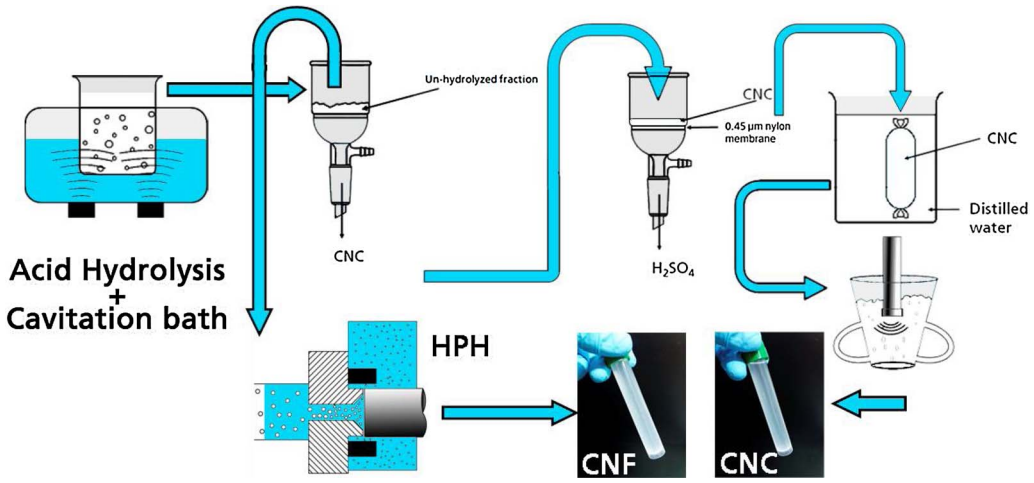

Fig. 1. Visual flowchart of the CNF/CNC production processes.

suspension (1:100 g: mL) and then passed several times through a homogenizer by increasing the pressure until ~1000 bar were achieved at which suspension was passed with constant flow-rate during 90 min. CNF suspensions were adjusted to 5 wt% and kept at 5 °C.

2.4. Fiber characterization

Chemical analysis of the blue agave fibers was performed to determine the amount of cellulose available for further extraction. This characterization was carried out according to standard methods (TAPPI T204cm-07, 2007; TAPPI T207cm-08, 2008; TAPPI T222 om-11, 2011; TAPPI T211 om-12, 2012; Wise, Murphy, & D'Addieco, 1946). Infrared spectra were recorded on a PerkinElmer Spectrum Two FT-IR Spectrometer equipped with a Universal ATR accessory with internal reflection diamond crystal lens. The defined range was from 600 to 4000 cm^{-1} and the resolution 8 cm^{-1}. For each sample, 20 scans were recorded. Color properties of the different treatments were measured with an X-Rite 500 series colorimeter over 10 different regions of each composite, RGB profile was made for the final surface layer of each composite. SEM images were obtained with a Scanning electron microscope JEOL JSM-6400 with field emission cathode, with a lateral resolution of 10–11 Å at 20 kV.

2.5. Nanocellulose characterization

Cellulose nanoparticles were dry measured to control the yield of each treatment after hydrolysis by using Eq. (1):

$$Y = \frac{M_C \times M_T}{M_S \times M_O} \tag{1}$$

Where M_C is the mass of dried cellulose nanoparticles (Freeze-dried and then kept inside a desiccator); M_T is the mass of the total suspension, M_S is the mass of the suspension sample before drying and M_O is the cellulose mass before hydrolysis (CNC) or homogenizing (CNF).

Atomic force microscopy images were obtained operating in tapping mode with a NanoScope IIIa, Multimode TM-AFM from Digital Instruments-Veeco scanning probe microscope equipped with an integrated silicon tip cantilever with a resonance frequency of 300 kHz. To obtain representative results, different regions of the samples were scanned.

Particle size and zeta potential were measured inside Malvern Z nanosizer equipment, the refractive index for cellulose was considered at 1.47, measurements were performed at 25 °C. For size analysis, 0.1 g/L of cellulose suspension were put inside a disposable plastic cuvette performing 13 scans with an incidence angle of 173° repeated three times for each sample. For zeta potential nanocrystal suspensions were put inside Malvern folded capillary zeta cell and measured using the Smoluchowski model (κ·a = 1.50) 10 scans were performed and 3 specimens of each sample were measured (von Smoluchowski, 1903).

X-ray powder diffraction was measured to evaluate the crystallinity of the nanocellulose samples; patterns were collected with a Panalytical Phillips X'Pert PRO multipurpose diffractometer, with samples mounted on a zero background silicon wafer fixed in a generic sample holder, using monochromatic CuK_α radiation (λ = 1.5418 Å) in a 2θ range from 5 to 50 with step size of 0.026 and 80 s per step of at room temperature. Cellulose crystallinity was measured from the powder diffraction by using the Segal method, this method is easily implemented with data from a powder diffractometer, and despite the objections, it is still widely used as it constitutes a fast and easy tool to analyze and compare qualitatively different cellulose structures (French & Santiago Cintrón, 2013). To achieve this index, the I_{200} diffraction, which is associated with the main crystalline domain, and the maximum of the scatter of the amorphous cellulose, which has its highest intensity around 2θ = 18° are used. Segal relative crystallinity index is given by the following equation:

$$\mathrm{Cr.I._{Segal}} = 100 \times \frac{I_{200} - I_{AM}}{I_{tot}} \tag{2}$$

For a more reliable crystallinity index, peak fitting method was used to determine the ratio of the fitted crystalline area to the total reflection area including the amorphous contribution with the extracted background (Wada & Okano, 2001). Selected peaks correspond to the 1–10, 110, 200 and 004 Miller indices corresponding to cellulose Iβ monoclinic unit cell. Apparent crystallinity was estimated with Eq. (3):

$$\mathrm{Cr.I._{Peak\ fitting}} = 100 \times \frac{\int_{2\theta_1}^{2\theta_2} S_{1\bar{1}0}\, d2\theta + \int_{2\theta_1}^{2\theta_2} S_{110}\, d2\theta + \int_{2\theta_1}^{2\theta_2} S_{200}\, d2\theta + \int_{2\theta_1}^{2\theta_2} S_{004}\, d2\theta}{\int_{d2_\theta}^{d2_\theta} S_{tot}\, d2\theta} \tag{3}$$

In which the sum of the areas correspondent to the diffraction of crystalline planes is assumed to be the area of the crystalline region, being $2\theta_1$ and $2\theta_2$ the limits of the fitted signal for the corresponding crystalline domains ($S_{1\text{-}10}$, S_{110}, S_{200}, S_{004}); while S_{tot} corresponds to the total area (Ahvenainen, Kontro, & Svedström, 2016; Hult, Iversen, & Sugiyama, 2003; Terinte, Ibbett, & Schuster, 2011). Least square iterations were done until coefficient of determination $R^2 \geq 0.997$ was achieved, which corresponds to a 99.7% accurate fitting.

Crystallite domain sizes were estimated with the Scherrer equation using the peaks corresponding to the crystalline regions as given by Eq. (4):

$$d_{hkl} = \frac{\kappa\lambda}{H_{hkl}\cos\theta} \tag{4}$$

With κ being the Scherrer constant most adjusted to the nanocrystal shape (0.86), λ the wavelength (1.5418 Å), H_{hkl} corresponds to the breadth or full width at half maximum intensity (FWHM) for the corresponding peak and θ is half the Bragg angle at peak maximum given in radians (Scherrer, 1918; Ungár & Gubicza, 2007; Warren, 1969).

The ^{13}C NMR spectrometry was performed using an AVANCE-500 Digital NMR spectrometer, at a frequency of 250 MHz with an acquisition time of 0.011 s, at room temperature. The spectrum was recorded over 32 scans and water was used as a solvent for all the nanocelluloses. The NMR crystallinity index was determined by separating the C_4 region of the spectrum into crystalline and amorphous peaks, and calculated by dividing the area of the crystalline peak by the total area assigned to the C_4 peak as shown in Eq. (5):

$$Cr.I._{NMR} = 100 \times \frac{\int_{87}^{93} Sdx}{\int_{80}^{93} Sdx} \quad (5)$$

In which S represents the intensity at a given chemical shift F(δ); x corresponds to the chemical shift, the crystalline assignment for the C_4 region was considered the region between 87–93 ppm and the total C_4 region was set between 80 and 93 ppm (Newman, 2004).

3. Results and discussion

Fig. 2 show the chemical composition of blue agave bagasse and leaf fibers was determined by TAPPI standards and is presented fully in the supplementary data. Cellulose is the main component in both leaves (63.10%) and bagasse (54.60%), in bagasse fibers cellulose and hemicelluloses are lower in content due to the sugar degradation that occurs during the tequila production in which blue agave cores are milled and cooked, extracting a considerable part of the sugars for the further alcohol production (Arrazola and de, 1969), this also makes these results to differ from other chemical compositions evaluated for blue agave bagasse (Alonso-Gutiérrez and de la, 2005; Satyanarayana et al., 2013) as the extraction process and the maturity of the plant are unpredictable variables. On the other hand, cellulose from leaf fibers is similar to those reported by previous works (Iñiguez-Covarrubias et al., 2001; Satyanarayana et al., 2013), the high cellulose content and low lignin of the blue agave, in general, makes it a desirable cellulose source.

Scanning electron images of the raw material were acquired to analyze the morphology of the fibers (supplementary data); leave fibers present a rounded cross-section, while that of bagasse fibers is rather rectangular; this phenomenon is caused by the mechanical beating to which bagasse fibers are subjected during juice extraction (milling) during tequila production; however widths are within the same range, with an average width of 50 µm. Leaf fibers are longer (70–100 cm) while bagasse fibers rarely reach over 20 cm; color also differs as it is further analyzed.

Fig. 3 shows the infrared spectra of the bagasse and the leaf fibers through each treatment. It can be observed the gradual disappearance of wavenumbers that are characteristic to lignin; the main bands which intensity is lost are at ~1610 cm^{-1} corresponding to the aromatic ring vibration (C=C stretch), another aromatic ring vibration at ~1500 cm^{-1} and the C–C deformation at ~1450 cm^{-1}. On the other hand, bands that are characteristic of cellulose present a sharper definition, this is evident especially in case of the free ν(OH) band at 3500–3000 cm^{-1}, the groups at ~2900 $cm^{-1}$and ~2860 cm^{-1} corresponding to ν(C–H) and $\nu(CH_2)$ symmetrical stretching of cellulose. In the 1500–500 cm^{-1} region, it can be pointed the higher resolution of peaks at ~1335 cm^{-1}, corresponding to glycosidic ν(C–O–C), ~1280 cm^{-1} of $\delta(CH_2)$ bending of crystalline cellulose (Garside & Wyeth, 2003; Xu, Yu, Tesso, Dowell, & Wang, 2013).

In Fig. 4 the process yields after each process are presented as the output of solid matter after each process divided by the input of solid. For a better understanding of the cellulose recovering, two more yields are displayed: the overall yield (Oy) which is the total amount of cellulose obtained from each gram of fibers and was 40% for bagasse and 51% for leaves, and the relative yield (Ry) which is the relation between the overall yield and the amount of cellulose present in the raw material as calculated by TAPPI standards. Ry shows that after O_T and TCF it was recovered the 72% of the cellulose present in the bagasse and 81% of the cellulose of the leaf fibers, with mayor cellulose losses occurring during O_T and the double oxygen stage, as high temperatures and the presence of sodium hydroxide may have depolymerized cellulose chains to glucose. O_T yields are in both cases higher than those obtained in similar works, which have been reported around 50% (Palomo-Briones et al., 2017; Pérez-Pimienta et al., 2017). Process yields at peroxide stages (P_Q and P_O) are above 90% mainly because the mayor lignin and hemicellulosic fractions have been already solubilized but also because of the lesser aggressiveness of these treatments to the cellulosic fibers.

Fig. 4 also shows the color properties of the fibers after each treatment along with their simulated solid color obtained from the resulting Lab coordinates. It is to highlight that the final cellulose fibers present good luminosity values (L*) which are 93.66 for the bagasse and 94.61 for the leaves, these results are above industrial requirements, which demand between 93 and 95 L*. Organosolv treatment darkened the color regarding the original material, this feature has been observed in similar works that use organosolv treatments on natural fibers (Watkins, Nuruddin, Hosur, Tcherbi-Narteh, & Jeelani, 2015) and it can be associated with the presence of polyphenolic chromophores originated from the ring-opening of lignin chains (Castellan & Grelier, 2016). Bleached bagasse had higher value for both a* and b* than leaf fibers (0.64 and 0.14 for a*, and 6.88 and 4.29 respectively), these

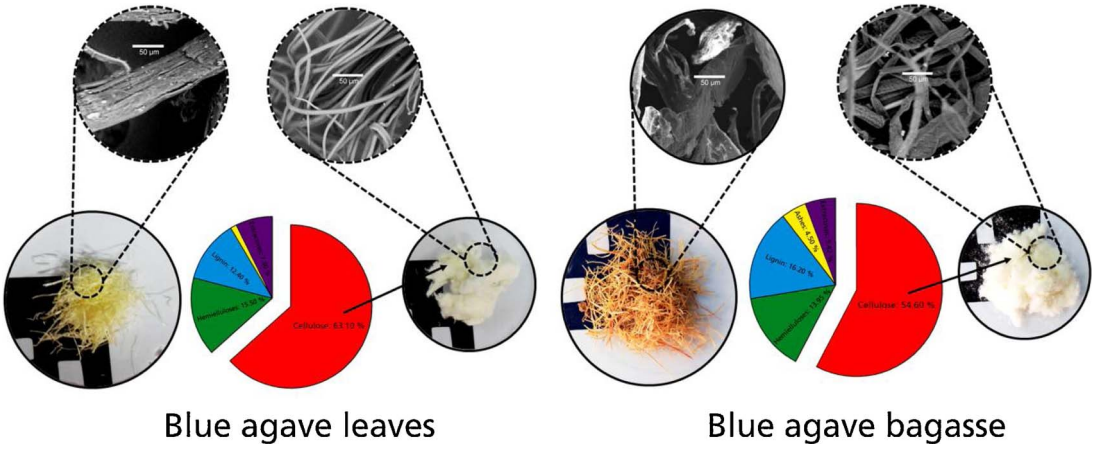

Fig. 2. Visual aspect and SEM images of the fibers before and after the bleaching.

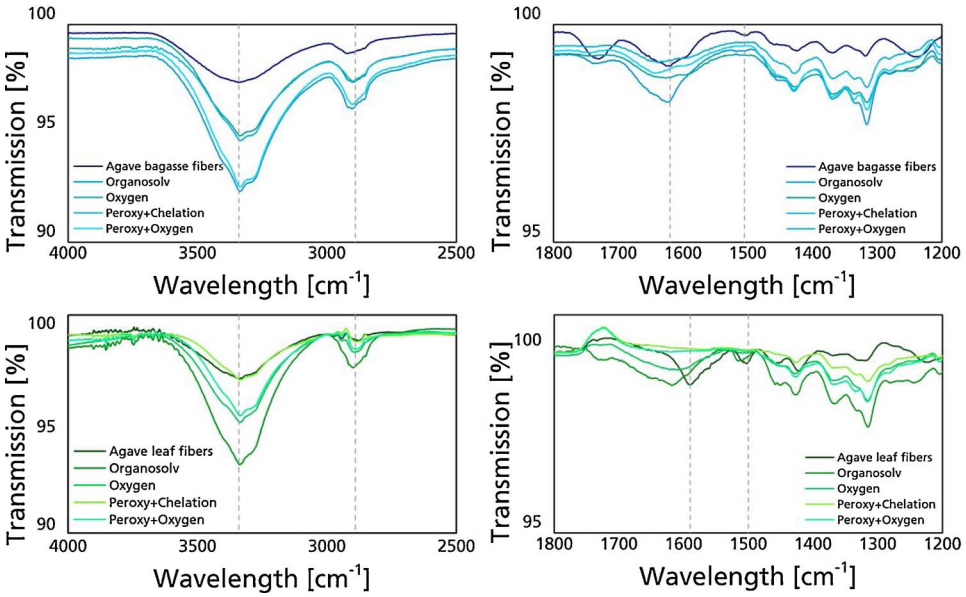

Fig. 3. Normalized FT-IR spectra of blue agave bagasse and leaf fibers through each step of the treatment. (For interpretation of the references to colour in this figure legend, the reader is referred to the web version of this article.)

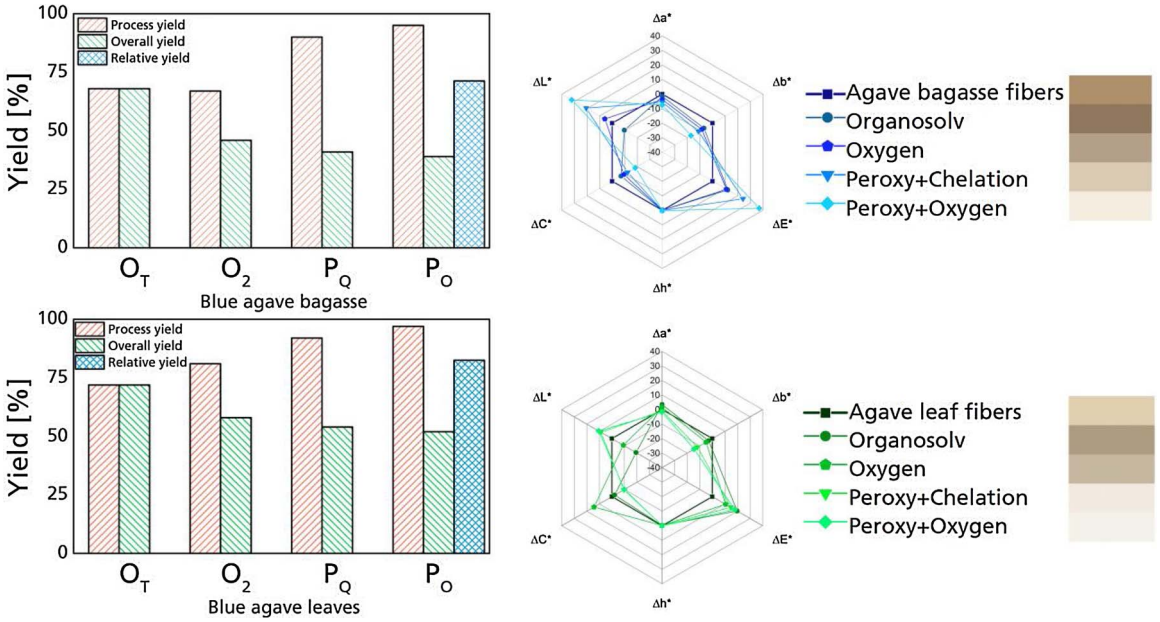

Fig. 4. Yields and color appearance parameters corresponding to Lab* space (ΔL*, Δa* and Δb*) as well as chrominance (ΔC*), hue (Δhab) and color difference (ΔE*) of blue agave bagasse (c) and blue agave leaves (d) through pulping and bleaching. Process yield corresponds to the yield after each process, overall yield corresponds to the amount of cellulose obtained related to the biomass used and relative yield corresponds to the obtained cellulose compared to the cellulose content as obtained from TAPPI methods. Beside each name the corresponding color solid is represented as simulated by RGB color space. (For interpretation of the references to colour in this figure legend, the reader is referred to the web version of this article.)

numbers (+a* and +b*) are related to red-yellow colors which can be due to either residual lignins or to chromophores appearing because of glucose oxidation (Castro et al., 2011; Mosca Conte et al., 2012). The initial darkening after organosolv is further reverted during bleaching, chroma presents reductions from initial values (25 for bagasse and 18 for leaves) which were further reduced (7 for bagasse and 4 for leaves) after bleaching, chroma is related to the intensity of colors, grayscale colors lack chroma as they are closer to the L^-/L^+ axis of the CIEL*-C*h*(a*b*) tridimensional space.

Fig. 5 shows AFM images of the obtained nanoparticles. During processes, bagasse fibers were easier to process either CNC or CNF, as the processes of tequila production eased the cellulose fractionation during both treatments and resulted, under identical conditions, in cellulose nanoparticles of smaller dimensions than those obtained from leaf fibers; this can be confirmed with size ranges presented in the lower part of Fig. 5, in which CNC_L and CNF_L present larger dimensions. The action of sulfuric acid in the cellulose fibers allowed the isolation of CNC with an average width of 33 ± 13 nm and length 350 ± 153 nm with a very homogeneous morphology, which is due to the retention of particles with bigger size by the Buchner filter funnel cellulose separation CNC_B are significantly smaller than CNC_L under the same conditions The use of hydrogen peroxide has been reported as an influential factor in the determination of fiber morphology after treatment, as it weakens the fiber structure by oxidizing low chain carbohydrates (Topalovic et al., 2007; Zeronian & Inglesby, 1995). While this situation is often counterproductive for pulp and fabrics, it makes TCF fibers desirable for nanocellulose production as the feasibility to obtain smaller fibers under same conditions makes them more competitive. In

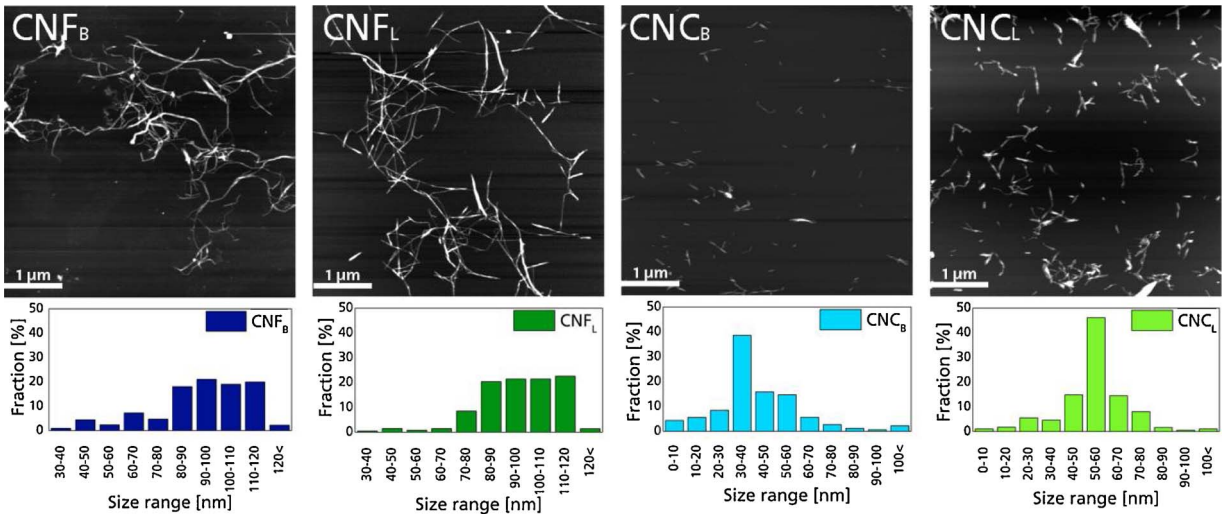

Fig. 5. AFM images of the elaborated cellulose nanoparticles. The lower part of the figure presents the corresponding size ranges as obtained with the Nanosizer.

case of CNF, the action of HPH allowed to tear microfibrillated cellulose into single nanofibers or groups of 2–3 nanofibers attached; in this case, shape is less constant as fibers are presented sometimes separated in one of their ends but still attached in the other (branching), this occurs because mechanical isolation methods do not eliminate amorphous cellulose that can still be left after the bleaching processes, anyhow the average length was 607 ± 85 nm and the average width 68 ± 22 nm.

Fig. 6 presents CNC and CNF yields (Oy and Ry) as obtained from Eq. (1), crystallinity indices, zeta potential (ζ_{POT}), and crystallite region sizes as approximated by Scherrer equation. Oy is the yield of cellulose nanoparticles after hydrolysis or homogenization and Ry is the yield of cellulose nanoparticles referred to the original cellulose content, this is important as this value shows the expected cellulose nanoparticles that can be obtained from the initial cellulose after cellulose loses or degradation after each treatment. As acid hydrolysis dissolves non-crystalline regions of the cellulose structures, yields of cellulose nanocrystals are lower than those of cellulose nanofibers, which in contrast present lower crystallinity indexes with either crystallinity evaluation method. Leaf fibers have the highest yields, with 93.84% for CNF_L and 60.84% for CNC_L, while CNC_B had 50.23% and CNF_B 86.24%. Bagasse fibers were less resistant to chemical hydrolysis and presented more degradation, as the auto-hydrolysis done during tequila production had already influenced the fiber morphology. It is to highlight that CNC yields obtained by passing the suspension through different sintered glass plates were between 50 and 60%, which is between the commonly referred yields (ranging between 5 or 6% up to 80% depending on the process and the source), but better than yields traditionally obtained via acid hydrolysis and centrifugation, which is between 20 and 40% (Trache, Hussin, Haafiz, & Thakur, 2017). Crystallinity index was calculated using Segal method ($Cr.I_{SM}$) which is the easiest way to qualify crystallinity indexes and therefore the most widely used but, as explained before, with low accuracy and, therefore crystallinity indices obtained with the peak fitting method ($Cr.I_{PF}$) and with NMR method ($Cr.I_{NMR}$) are also presented, as they represent more accurate crystallinity values. Crystalline indices show little differences between the different methods, but they concur with previous works in which Segal index is lower than that of peak method. In general, crystallinity shows higher indexes for CNC than for CNF obtained, which is related to the elimination of paracrystalline and amorphous cellulose during hydrolysis in which glucose chains are dissolved from the main fibrils. Zeta potential presented values that are characteristic of CNC and CNF respectively; with CNC presenting more stability than CNF because of residual sulfur particles attached to the −OH groups on the cellulose surface that may remain after hydrolysis (Abitbol, Kloser, & Gray, 2013). Previous works have also achieved stable cellulose nanoparticles (Han, Zhou, Wu, Liu, & Wu, 2013; Tonoli et al., 2012).

Normalized diffraction patterns (Fig. 7) show similar shapes which are similar to those published elsewhere for cellulose I crystalline

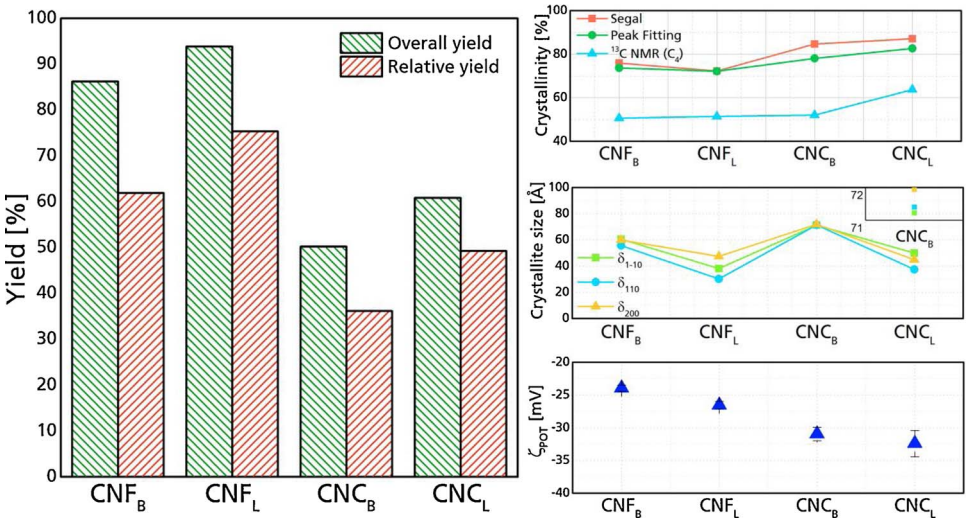

Fig. 6. Left: Yields of the elaborated nanoparticles, overall yield corresponds to the amount of CNC/CNF obtained for each 100 g of cellulose, relative yield corresponds to the amount of CNC/CNF obtained related to the cellulose content as calculated by TAPPI methods Right: Crystallinity indices, crystallite domain sizes and zeta potential of the elaborated nanoparticles.

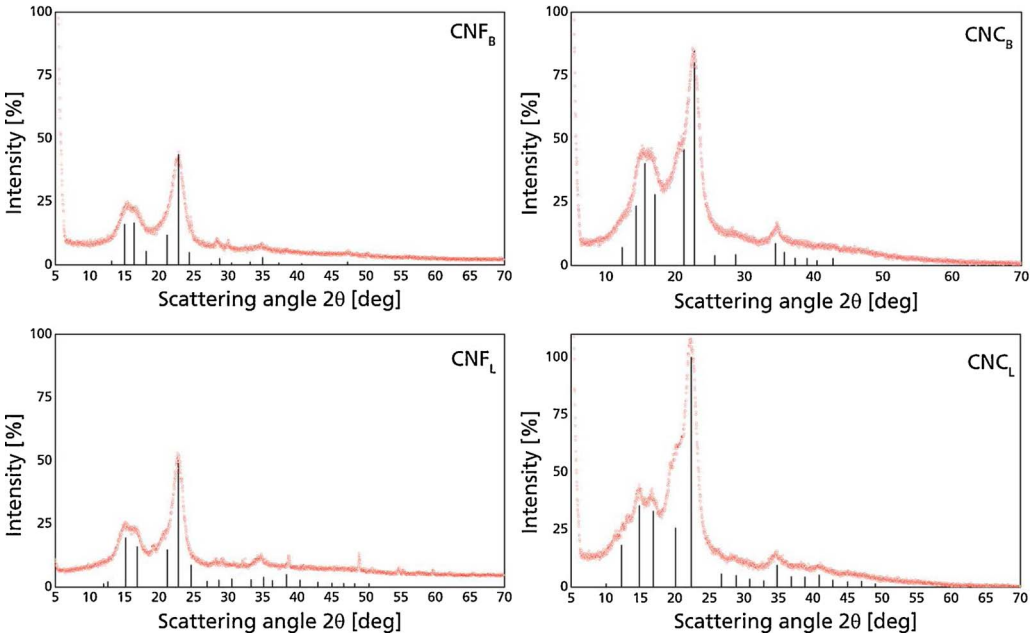

Fig. 7. Powder diffraction patterns (red scatter) as well as main diffraction signals as obtained from 2nd Derivate fitting (black lines) all values are normalized to the intensity of the 200 plane of the CNC_L. (For interpretation of the references to colour in this figure legend, the reader is referred to the web version of this article.)

allomorphs (Horikawa & Sugiyama, 2009) with two main overlapped signals at 2θ = 14–16° and 2θ = 20–24° and a small signal at 2θ–34°. Fitted curves showed peaks associated with cellulose corresponding to 1–10, 110, 200 and 004 crystalline planes, which are present in all the cases with different intensity and broadening. A general assumption for this analysis is that increased amorphous contribution is the main contributor to peak broadening. However, more than a crystalline disorder (amorphous content), there are other intrinsic factors that influence peak broadening, such as crystallite size and the anisotropy of the shape of the crystallites (Popa & Balzar, 2008)-not to be confused with an anisotropic distribution- as there have been reported non-uniform strains within the crystal (Park, Baker, Himmel, Parilla, & Johnson, 2010). However, the presence of hidden 'humps' or 'halos' which is more visible in CNF, is without any doubt due to amorphous presence. CNC samples have more defined shapes with the peak due to 200 plane being well defined and broad (smaller crystallites) while CNF have scattered diffractions with more differences between each other; and the characteristic halo between 2θ = 10–15°, which corresponds to low-crystalline cellulose as it has been stated in other works, this typical 'hump' starts at 2θ ~ 12° and has its main height at 2θ ~ 19.92° which corresponds to typical amorphous contribution of native cellulose (Boissou et al., 2014).

Nuclear magnetic resonance chemical shifts are presented in Fig. 8, most of them correspond to nanocellulose NMR reported by other researches (Lee et al., 2013), however, it is difficult to compare results as the spectral morphology and particularities differ from species to species (Kono et al., 2002). CNC_L signal has a different shape in the C_4 and C_6 regions, with a less intense signal in the accessible fibril surface region (80–90 ppm) and with the Iα and Iβ peaks more pronounced, which may imply a reduction in the paracrystalline region, which can be corroborated with the Cr.I in Fig. 4. On the other hand, the amorphous C_6 region has a double peak with increased intensity than that of the crystalline region (61–63 ppm). CNC_L chemical shifts also present some similarities with Cellulose II NMR analysis, especially in case of the C_1 double peak which is not present in the rest of the signals (Mittal, Katahira, Himmel, & Johnson, 2011); this presence of Cellulose II is also seen in the XRD (peak at ~12° 2θ) and it might be attributed to amorphous cellulose I being dissolved during the acid hydrolysis.

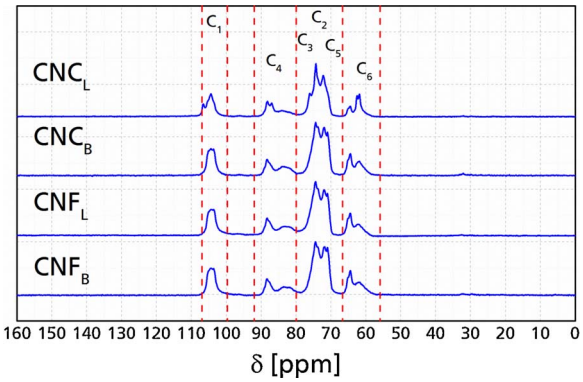

Fig. 8. NMR analysis of cellulose nanoparticles.

4. Conclusions

Native cellulose was extracted from byproducts generated during tequila production with processes known by their low environmental impact but which are not widely used because of the properties which traditionally attributed to those processes by the industry. However, to elaborate CNF and CNF, the use of organosolv and TCF resulted in fibers with high potential. Cellulose nanoparticles obtained from such celluloses resulted in high production yields (particularly in case of CNC), while their analyzed properties were within the expected criteria (dimensions, colloidal stability, and crystallinity) and represent a suitable valorization for rather undervalued side-streams. Differences between bagasse fibers and leave fibers are visible at large scale, but as the fiber size is reduced, these differences decrease significantly. Therefore, blue agave byproducts are a good source to produce value-added products as cellulose nanocrystals and cellulose nanofibers from either leaves or bagasse.

Acknowledgments

The authors would like to acknowledge the University of the Basque Country (UPV/EHU) through grant PIF 13/050, Basque Government (IT1008-16), the Federal Agency for Support and Evaluation of Graduate Education (CAPES) through process BEX8710/14-7 and Mexican Council of Science and Technology (CONACyT), through scholarship No. 216178 for financially supporting this work. The authors thank Dr. Miren Arrese for her help and guidance with the

homogenizer Dr. Maite Insausti and Dr. Oihane Arriortua for their kind help and support with Nanosizer and SGIker of UPV/EHU for technical and human support provided with XRD, NMR, and AFM characterizations.

References

Abitbol, T., Kloser, E., & Gray, D. G. (2013). Estimation of the surface sulfur content of cellulose nanocrystals prepared by sulfuric acid hydrolysis. *Cellulose, 20*(2), 785–794. http://dx.doi.org/10.1007/s10570-013-9871-0.

Ahvenainen, P., Kontro, I., & Svedström, K. (2016). Comparison of sample crystallinity determination methods by X-ray diffraction for challenging cellulose I materials. *Cellulose, 23*(2), 1073–1086. http://dx.doi.org/10.1007/s10570-016-0881-6.

Alonso, J. L., Parajó, J. C., & Yáñez, R. (2003). Totally chlorine free bleaching of organosolv pulps. *Journal of Wood Chemistry and Technology, 23*(2), 161–178. http://dx.doi.org/10.1081/WCT-120021923.

Alonso-Gutiérrez, M., & de la, S. (2005). *Valorisation de la bagasse de l'agave tequilana W. cv azul: caractérisation, étude de la digestibilité et de la fermentation des sucres.* Institut National Polythechnique de Toulouse.

Aranda-García, F. J., González-Núñez, R., Jasso-Gastinel, C. F., & Mendizábal, E. (2015). Water absorption and thermomechanical characterization of extruded starch/poly (lactic acid)/agave bagasse fiber bioplastic composites. *International Journal of Polymer Science, 2015*, 1–7. http://dx.doi.org/10.1155/2015/343294.

Arrazola, D. F., & de, M. (1969). *Estudio del Contenido de Azúcares en la Piña del Agave tequilana.* Universidad Autónoma de Puebla.

Bajpai, P. (2004). Biological bleaching of chemical pulps. *Critical Reviews in Biotechnology, 24*(1), 1–58. http://dx.doi.org/10.1080/07388550490465817.

Barbosa, A., Robles, E., Ribeiro, J., Lund, R., Carreño, N., & Labidi, J. (2016). Cellulose nanocrystal membranes as excipients for drug delivery systems. *Materials, 9*(12), 1002. http://dx.doi.org/10.3390/ma9121002.

Boissou, F., Mühlbauer, A., De Oliveira Vigier, K., Leclercq, L., Kunz, W., Marinkovic, S., ... Jérôme, F. (2014). Transition of cellulose crystalline structure in biodegradable mixtures of renewably-sourced levulinate alkyl ammonium ionic liquids, γ-valerolactone and water. *Green Chemistry, 16*(5), 2463. http://dx.doi.org/10.1039/c3gc42396d.

Castellan, A., & Grelier, S. (2016). *Color and color reversion of cellulosic and lignocellulosic fibers. Lignocellulosic fibers and wood handbook*. Hoboken, NJ, USA: John Wiley & Sons, Inc531–551. http://dx.doi.org/10.1002/9781118773727.c.

Castro, K., Princi, E., Proietti, N., Manso, M., Capitani, D., Vicini, S., ... De Carvalho, M. L. (2011). Assessment of the weathering effects on cellulose based materials through a multianalytical approach. *Nuclear Instruments and Methods in Physics Research Section B: Beam Interactions with Materials and Atoms, 269*(12), 1401–1410. http://dx.doi.org/10.1016/j.nimb.2011.03.027.

Chen, W., Yu, H., Liu, Y., Chen, P., Zhang, M., & Hai, Y. (2011). Individualization of cellulose nanofibers from wood using high-intensity ultrasonication combined with chemical pretreatments. *Carbohydrate Polymers, 83*(4), 1804–1811. http://dx.doi.org/10.1016/j.carbpol.2010.10.040.

Eichhorn, S. J. (2011). Cellulose nanowhiskers: Promising materials for advanced applications. *Soft Matter, 7*(2), 303. http://dx.doi.org/10.1039/c0sm00142b.

Espino, E., Cakir, M., Domenek, S., Román-Gutiérrez, A. D., Belgacem, N., & Bras, J. (2014). Isolation and characterization of cellulose nanocrystals from industrial by-products of Agave tequilana and barley. *Industrial Crops and Products, 62*, 552–559. http://dx.doi.org/10.1016/j.indcrop.2014.09.017.

Fernández-Rodríguez, J., Gordobil, O., Robles, E., González-Alriols, M., & Labidi, J. (2017). Lignin valorization from side-streams produced during agricultural waste pulping and total chlorine free bleaching. *Journal of Cleaner Production, 142*, 2609–2617. http://dx.doi.org/10.1016/j.jclepro.2016.10.198.

Fillat, Ú., Wicklein, B., Martín-Sampedro, R., Ibarra, D., Ruiz-Hitzky, E., Valencia, C., ... Eugenio, M. E. (2017). Assessing cellulose nanofiber production from olive tree pruning residue. *Carbohydrate Polymers, 179*(1), http://dx.doi.org/10.1016/j.carbpol.2017.09.072.

French, A. D., & Santiago Cintrón, M. (2013). Cellulose polymorphy, crystallite size, and the Segal Crystallinity Index. *Cellulose, 20*(1), 583–588. http://dx.doi.org/10.1007/s10570-012-9833-y.

García, A., Gandini, A., Labidi, J., Belgacem, N., & Bras, J. (2016). Industrial and crop wastes: A new source for nanocellulose biorefinery. *Industrial Crops and Products, 93*, 26–38. http://dx.doi.org/10.1016/j.indcrop.2016.06.004.

Garcia de Rodriguez, N. L., Thielemans, W., & Dufresne, A. (2006). Sisal cellulose whiskers reinforced polyvinyl acetate nanocomposites. *Cellulose, 13*(3), 261–270. http://dx.doi.org/10.1007/s10570-005-9039-7.

Garside, P., & Wyeth, P. (2003). Identification of cellulosic fibres by FTIR spectroscopy – thread and single fibre analysis by attenuated total reflectance. *Studies in Conservation, 48*(4), 269–275. http://dx.doi.org/10.1179/sic.2003.48.4.269.

Gatenholm, P., & Klemm, D. (2010). Bacterial nanocellulose as a renewable material for biomedical applications. *MRS Bulletin, 35*, 208–213. http://dx.doi.org/10.1557/mrs2010.653.

Gellerstedt, G., & Pettersson, I. (1982). Hemical aspects of hydrogen peroxide bleaching. Part II the bleaching of kraft pulps. *Journal of Wood Chemistry and Technology, 2*(3), 231–250. http://dx.doi.org/10.1080/02773818208085133.

Gierer, J. (1982). Chemistry of delignification. *Wood Science and Technology, 36*(1), 289–312. http://dx.doi.org/10.1007/BF00350807.

Gordobil, O., Egüés, I., Llano-Ponte, R., & Labidi, J. (2014). Physicochemical properties of PLA lignin blends. *Polymer Degradation and Stability,* 1–9. http://dx.doi.org/10.1016/j.polymdegradstab.2014.01.002.

Guo, J., Guo, X., Wang, S., & Yin, Y. (2016). Effects of ultrasonic treatment during acid hydrolysis on the yield, particle size and structure of cellulose nanocrystals. *Carbohydrate Polymers, 135*, 248–255. http://dx.doi.org/10.1016/J.CARBPOL.2015.08.068.

Han, J., Zhou, C., Wu, Y., Liu, F., & Wu, Q. (2013). Self-assembling behavior of cellulose nanoparticles during freeze- drying: Effect of suspension concentration, particle size, crystal structure and surface charge. *Biomacromolecules, 14*(5), 1529–1540.

Henriksson, M., Henriksson, G., Berglund, L. A., & Lindström, T. (2007). An environmentally friendly method for enzyme-assisted preparation of microfibrillated cellulose (MFC) nanofibers. *European Polymer Journal, 43*(8), 3434–3441. http://dx.doi.org/10.1016/j.eurpolymj.2007.05.038.

Herrera, A., Téllez-Luis, S. J., González-Cabriales, J. J., Ramírez, J. A., & Vázquez, M. (2004). Effect of the hydrochloric acid concentration on the hydrolysis of sorghum straw at atmospheric pressure. *Journal of Food Engineering, 63*(1), 103–109. http://dx.doi.org/10.1016/S0260-8774(03)00288-7.

Hettrich, K., Pinnow, M., Volkert, B., Passauer, L., & Fischer, S. (2014). Novel aspects of nanocellulose. *Cellulose, 21*(4), 2479–2488. http://dx.doi.org/10.1007/s10570-014-0265-8.

Horikawa, Y., & Sugiyama, J. (2009). Localization of crystalline allomorphs in cellulose microfibril. *Biomacromolecules, 10*(8), 2235–2239. http://dx.doi.org/10.1021/bm900413k.

Hult, E. L., Iversen, T., & Sugiyama, J. (2003). Characterization of the supermolecular structure of cellulose in wood pulp fibres. *Cellulose, 10*(2), 103–110. http://dx.doi.org/10.1023/A.;1;1024080700873.

Iñiguez-Covarrubias, G., Díaz-Teres, R., Sanjuan-Dueñas, R., Anzaldo-Hernández, J., & Rowell, R. M. (2001). Utilization of by-products from the tequila industry. Part 2: Potential value of Agave tequilana Weber azul leaves. *Bioresource Technology, 77*(2), 101–108. http://dx.doi.org/10.1016/S0960-8524(00)00167-X.

Ibarra, D., Camarero, S., Romero, J., Martínez, M. J., & Martínez, A. T. (2006). Integrating laccase–mediator treatment into an industrial-type sequence for totally chlorine-free bleaching of eucalypt kraft pulp. *Journal of Chemical Technology & Biotechnology, 81*(7), 1159–1165. http://dx.doi.org/10.1002/jctb.1485.

Idarraga, G., Ramos, J., Zuñiga, V., Sahin, T., & Young, R. A. (1999). Pulp and paper from blue agave waste from tequila production. *Journal of Agricultural and Food Chemistry, 47*(10), 4450–4455. http://dx.doi.org/10.1021/JF990045N.

Iwamoto, S., Abe, K., & Yano, H. (2008). The effect of hemicelluloses on wood pulp nanofibrillation and nanofiber network characteristics. *Biomacromolecules, 9*(3), 1022–1026. http://dx.doi.org/10.1021/bm701157n.

Jonoobi, M., Harun, J., Shakeri, A., Misra, M., & Oksman, K. (2009). Chemical composition, crystallinity, and thermal degradation of bleached and unbleached kenaf bast (Hibiscus cannabinus) pulp and nanofibers. *BioResources, 4*(2), 626–639.

Kono, H., Yunoki, S., Shikano, T., Fujiwara, M., Erata, T., & Takai, M. (2002). CP/MAS 13C NMR study of cellulose and cellulose derivatives. 1. Complete assignment of the CP/MAS 13C NMR spectrum of the native cellulose. *Journal of the Chemical Society, 124*(5), 7506–7511. http://dx.doi.org/10.1021/JA010704O.

Lachenal, D., Chirat, C., Benattar, N., Hamzeh, Y., Mateo, C., & Brochier, B. (2005). Influence of pulp colour on bleachability. Ways to improve the bleaching response of alkaline pulp. *ATIP. Association Technique de L'Industrie Papetiere, 59*(3), 6–11.

Lavoine, N., Desloges, I., Dufresne, A., & Bras, J. (2012). Microfibrillated cellulose – its barrier properties and applications in cellulosic materials: A review. *Carbohydrate Polymers, 90*(2), 735–764. http://dx.doi.org/10.1016/j.carbpol.2012.05.026.

Lee, S. Y., Chun, S. J., Kang, I. A., & Park, J. Y. (2009). Preparation of cellulose nanofibrils by high-pressure homogenizer and cellulose-based composite films. *Journal of Industrial and Engineering Chemistry, 15*(1), 50–55. http://dx.doi.org/10.1016/j.jiec.2008.07.008.

Lee, C. M., Mittal, A., Barnette, A. L., Kafle, K., Park, Y. B., Shin, H., ... Kim, S. H. (2013). Cellulose polymorphism study with sum-frequency-generation (SFG) vibration spectroscopy: Identification of exocyclic CH2OH conformation and chain orientation. *Cellulose, 20*(3), 991–1000. http://dx.doi.org/10.1007/s10570-013-9917-3.

Li, L., Lee, S., Lee, H. L., & Youn, H. J. (2011). Hydrogen peroxide bleaching of hardwood kraft pulp with adsorbed birch xylan and its effect on paper properties. *BioResources, 6*(1), 721–736.

Mateo, C., Chirat, C., & Lachenal, D. (2005). The chromophores remaining after bleaching to moderate brightness. *Journal of Wood Chemistry and Technology, 24*(3), 279–288. http://dx.doi.org/10.1081/WCT-200038192.

Mittal, A., Katahira, R., Himmel, M. E., & Johnson, D. K. (2011). Effects of alkaline or liquid-ammonia treatment on crystalline cellulose: Changes in crystalline structure and effects on enzymatic digestibility. *Biotechnology for Biofuels, 4*(1), 41. http://dx.doi.org/10.1186/1754-6834-4-41.

Morán, J. I., Alvarez, V.a., Cyras, V. P., & Vázquez, A. (2008). Extraction of cellulose and preparation of nanocellulose from sisal fibers. *Cellulose, 15*(1), 149–159. http://dx.doi.org/10.1007/s10570-007-9145-9.

Mosca Conte, A., Pulci, O., Knapik, A., Bagniuk, J., Del Sole, R., Lojewska, J., & Missori, M. (2012). Role of cellulose oxidation in the yellowing of ancient paper. *Physical Review Letters, 108*(15), 158301. http://dx.doi.org/10.1103/PhysRevLett.108.158301.

National Regulator Council for Tequila Industry (2017). *CRT.* Retrieved September 25, 2017, from: https://www.crt.org.mx/.

Nelson, P. J. (1998). Elemental chlorine free (ECF) and totally chlorine free (TCF) bleaching of pulps. In R. A. Young (Ed.). *Environmentally friendly technologies for the pulp and paper industry*. San Francisco, CA: John Wiley & Sons, Inc.

Newman, R. H. (2004). Homogeneity in cellulose crystallinity between samples of Pinus radiata wood. *Holzforschung, 58*(1), 91–96. http://dx.doi.org/10.1515/HF.;1;2004.012.

Pérez-Pimienta, J. A., Vargas-Tah, A., López-Ortega, K. M., Medina-López, Y. N., Mendoza-Pérez, J. A., Avila, S., ... Martinez, A. (2017). Sequential enzymatic

saccharification and fermentation of ionic liquid and organosolv pretreated agave bagasse for ethanol production. *Bioresource Technology, 225*, 191–198. http://dx.doi.org/10.1016/j.biortech.2016.11.064.

Palomo-Briones, R., López-Gutiérrez, I., Islas-Lugo, F., Galindo-Hernández, K. L., Munguía-Aguilar, D., Rincón-Pérez, J. A., ... Razo-Flores, E. (2017). Agave bagasse biorefinery: Processing and perspectives. *Clean Technologies and Environmental Policy,* 1–19. http://dx.doi.org/10.1007/s10098-017-1421-2.

Park, S., Baker, J. O., Himmel, M. E., Parilla, P. A., & Johnson, D. K. (2010). Cellulose crystallinity index: Measurement techniques and their impact on interpreting cellulase performance. *Biotechnology for Biofuels, 3*(1), 10. http://dx.doi.org/10.1186/1754-6834-3-10.

Ponce-Reyes, C. E., Chanona-Pérez, J. J., Garibay-Febles, V., Palacios-González, E., Karamath, J., Terrés-Rojas, E., & Calderón-Domínguez, G. (2014). Preparation of cellulose nanoparticles from agave waste and its morphological and structural characterization. *Revista Mexicana de Ingeniería Química, 13*(3), 897–906. Retrieved from: http://www.scielo.org.mx/scielo.php?pid=S1665-27382014000300021&script=sci_arttext&tlng=en.

Popa, N. C., & Balzar, D. (2008). Size-broadening anisotropy in whole powder pattern fitting. Application to zinc oxide and interpretation of the apparent crystallites in terms of physical models. *Journal of Applied Crystallography, 41*(41), 615–627. http://dx.doi.org/10.1107/S0021889808012223.

Robles, E., Salaberria, A. M., Herrera, R., Fernandes, S. C. M., & Labidi, J. (2016). Self-bonded composite films based on cellulose nanofibers and chitin nanocrystals as antifungal materials. *Carbohydrate Polymers, 144*, 41–49. http://dx.doi.org/10.1016/j.carbpol.2016.02.024.

Süss, H. U., & Nimmerfroh, N. F. (1996). Hydrogen peroxide in chemical pulp bleaching. *Meeting on pulp bleaching* p. 15.

Satyanarayana, K. G., Flores-Sahagun, T. H. S., Dos Santos, L. P., Dos Santos, J., Mazzaro, I., & Mikowski, A. (2013). Characterization of blue agave bagasse fibers of Mexico. *Composites Part A: Applied Science and Manufacturing, 45*, 153–161. http://dx.doi.org/10.1016/j.compositesa.2012.09.001.

Scherrer, P. (1918). Bestimmung der Größe und der inneren Struktur von Kolloidteilchen mittels Röntgenstrahlen. *Nachrichten von Der Gesellschaft Der Wissenschaften Zu Göttingen Mathematisch-Physikalische Klasse, 1918*, 98–100.

Shatalov, A. A., & Pereira, H. (2007). Polysaccharide degradation during ozone-based TCF bleaching of non-wood organosolv pulps. *Carbohydrate Polymers, 67*(3), 275–281. http://dx.doi.org/10.1016/J.CARBPOL.;1;2006.05.028.

TAPPI T204cm-07 (2007). *Solvent extractives of wood and pulp. Standard by technical association of the pulp and paper industry* Atlanta, GA.

TAPPI T207cm-08 (2008). *Water solubility of wood and pulp. Standard by technical association of the pulp and paper industry* Atlanta, GA.

TAPPI T211 om-12 (2012). *Ash in wood, pulp, paper and paperboard: Combustion at 525 degrees. Standard by technical association of the pulp and paper industry* Atlanta, GA.

TAPPI T222 om-11 (2011). *Acid-insoluble lignin in wood and pulp. Standard by technical association of the pulp and paper industry* Atlanta, GA.

Terinte, N., Ibbett, R., & Schuster, K. C. (2011). Overview on native cellulose and microcrystalline cellulose I structure studied by X-Ray diffraction (Waxd): Comparison between measurement techniques. *Lenzinger Berichte, 89*, 118–131. http://dx.doi.org/10.1163/156856198X00740.

Tonoli, G. H. D., Teixeira, E. M., Corrêa, A. C., Marconcini, J. M., Caixeta, L. A., Pereira-Da-Silva, M. A., & Mattoso, L. H. C. (2012). Cellulose micro/nanofibres from Eucalyptus kraft pulp: Preparation and properties. *Carbohydrate Polymers, 89*(1), 80–88. http://dx.doi.org/10.1016/j.carbpol.2012.02.052.

Topalovic, T., Nierstrasz, V. A., Bautista, L., Jocic, D., Navarro, A., & Warmoeskerken, M. M. C. G. (2007). Analysis of the effects of catalytic bleaching on cotton. *Cellulose, 14*(4), 385–400. http://dx.doi.org/10.1007/s10570-007-9120-5.

Trache, D., Hussin, M. H., Haafiz, M. K. M., & Thakur, V. K. (2017). Recent progress in cellulose nanocrystals: Sources and production. *Nanoscale, 9*(5), 1763–1786. http://dx.doi.org/10.1039/C6NR09494E.

Tronc, E., Hernández-Escobar, C. A., Ibarra-Gómez, R., Estrada-Monje, A., Navarrete-Bolaños, J., & Zaragoza-Contreras, E. A. (2007). Blue agave fiber esterification for the reinforcement of thermoplastic composites. *Carbohydrate Polymers, 67*(2), 245–255. http://dx.doi.org/10.1016/j.carbpol.2006.05.027.

Ungár, T., & Gubicza, J. (2007). Nanocrystalline materials studied by powder diffraction line profile analysis. *Zeitschrift Für Kristallographie, 222*(3–4), 114–128. http://dx.doi.org/10.1524/zkri.2007.222. 3-4.114.

von Smoluchowski, M. (1903). Contribution to the theory of electro-osmosis and related phenomena. *Bulletin International de l'Academie Des Sciences de Cracovie, 3*(184).

Wada, M., & Okano, T. (2001). Localization of Iα and Iβ phases in algal cellulose revealed by acid treatments. *Cellulose, 8*, 183–188.

Warren, B. (1969). *X-ray diffraction.* Reading, USA: Addison-Wesley Pub. Co.

Watkins, D., Nuruddin, M., Hosur, M., Tcherbi-Narteh, A., & Jeelani, S. (2015). Extraction and characterization of lignin from different biomass resources. *Journal of Materials Research and Technology, 4*(1), 26–32. http://dx.doi.org/10.1016/j.jmrt.2014.10.009.

Wise, L. E., Murphy, M., & D'Addieco, A. A. (1946). Chlorite holocellulose, its fractionation and bearing on summative wood analysis and on studies on the hemicelluloses. *Paper Trade Journal, 122*(6), 35–43.

Xu, F., Yu, J., Tesso, T., Dowell, F., & Wang, D. (2013). Qualitative and quantitative analysis of lignocellulosic biomass using infrared techniques: A mini-review. *Applied Energy, 104*, 801–809. http://dx.doi.org/10.1016/j.apenergy.2012.12.019.

Zeronian, S. H., & Inglesby, M. K. (1995). Bleaching of cellulose by hydrogen peroxide. *Cellulose, 2*(4), 265–272. http://dx.doi.org/10.1007/BF00811817.